Journal of Oceanography, Vol. 64, pp. 495 to 509, 2008

Inertial Oscillations as Deep Ocean Response to Hurricanes

EUGENE G. MOROZOV[1,2] and MANUEL G. VELARDE[2]*

[1]*Shirshov Institute of Oceanology, Russian Academy of Sciences, Nakhimovsky prospekt 36, 117851 Moscow, Russia*
[2]*Instituto Pluridisciplinar, Paseo Juan XXIII No. 1, 28040 Madrid, Spain*

(Received 31 May 2007; in revised form 18 February 2008; accepted 18 February 2008)

We discuss the deep ocean response to passing hurricanes (*aka* typhoons), which are considered as generators of near-inertial, internal waves. The analysis of data collected in the northwestern parts of the Pacific and Atlantic oceans in the hurricane season permit us to assess the deep ocean response to such a strong atmospheric forcing. A large number of moorings (more than 100) in the northwestern Pacific have allowed us to characterize the spatial features of the oceanic response to typhoons and the variable downward velocity of near-inertial wave propagation. The velocity of their downward propagation varies in the range 1–10 m/hour. It is higher in the regions of low stratification and high anticyclonic vorticity. The inertial oscillations generated by a hurricane last for 10–12 days. The mean anticyclonic vorticity in the region increases the effective frequency of inertial oscillations by 0.001–0.004 cyc/hour.

Keywords:
· Typhoon,
· hurricane,
· inertial oscillations,
· near-inertial,
· internal waves.

1. Introduction

Near-internal waves with frequencies close to inertial are generated as a response of the ocean to wind forcing (Kundu, 1984; Shay and Elsberry, 1987; Brink, 1989). Asymmetric cooling of the upper layer, mixing, and near-inertial wave generation are the main processes that follow hurricane propagation (Church *et al*., 1989). (N.B.: Hurricanes in the Atlantic Ocean and typhoons in the Pacific). A propagating hurricane absorbs thermal energy from the warm ocean and intensifies (Shay *et al*., 2000). Warming of the atmosphere due to the cooling ocean and increasing density gradients cause stronger winds, when the hurricane propagates over a warm ocean. At the same time, the hurricane loses its energy because mechanical energy is transferred from the hurricane winds to the ocean, which causes mixing and generation of near-inertial, internal waves. Thus, a hurricane serves as a converter of the thermal energy to mechanical energy in the ocean.

Relative vorticity $\xi = \partial U/\partial y - \partial V/\partial x$ induced by flows with horizontal shear modulates the local Coriolis frequency f to the effective Coriolis frequency (or vorticity-modified Coriolis parameter) as $f_{eff} = \sqrt{f(f+\xi)}$ (Healey and LeBlond, 1969; Mooers, 1975; Kunze 1985; Kunze and Boss, 1998) or approximately $f_{eff} = f + \xi/2$. Since the component of the vector of the Earth's rotation normal to the surface and vector of anticyclonic vorticity are of opposite direction, relative vorticity reduces the Coriolis parameter. The vectors of anticyclonic vorticity ($\xi < 0$) and inertial rotation have the same sign; hence vorticity increases the frequency of inertial oscillations. Thus, the bandwidth of these oscillations increases compared to zero background vorticity.

Young and Ben Jelloul (1997) analyzed the propagation of near-inertial oscillations through a 3D field of smaller scale geostrophic eddies. They obtained solutions for energy refraction by the currents of eddies and analyzed wave dispersion, advection by geostrophic velocity, and refraction. The $\xi/2$ frequency shift is not expressed directly in the wave field due to cancellation of positive and negative vorticities ξ in the eddy field. Instead, the $\xi/2$ frequency shift is rectified to produce an average dispersive effect. The near-inertial oscillations have a frequency shift $-Kf_0k_z^2/N^2$, where K is average kinetic energy density of the geostrophic eddies, k_z is vertical wavenumber of near-inertial oscillations. No energy exchange is assumed between inertial oscillations and the flow.

van Meurs (1998) analyzed satellite-tracked, mixed-layer drifter data to study the temporal and spatial vari-

* Corresponding author. E-mail: mgvelarde@pluri.ucm.es

ability in the near-inertial currents of the surface mixed layer. Near-inertial currents interact with the mesoscale vorticity. Using a three-dimensional model the author showed that areas of large gradients in the mesoscale vorticity coincide with areas of low near-inertial energy.

Klein *et al*. (2004) proposed an analytical solution for the evolution of the spatial variability of wind-forced inertial energy in the upper ocean in the presence of an oceanic mesoscale eddy field. They found that within a few days the eddies efficiently reorganize an initially uniform kinetic energy field of near-inertial oscillations so that the spatial heterogeneity of the inertial energy resembles neither the vorticity nor the stream function, as previous studies had suggested, but the Laplacian of the vorticity.

The properties of internal waves with frequencies close to inertial differ from the rest of the frequency spectrum (Garrett, 2001). Their energy level is more variable than the level of internal waves with tidal and higher frequencies because they are subjected to the direct influence of wind forcing from the surface.

The downward propagating waves are associated with clockwise rotations (Brooks, 1983; Pinkel, 1984). Propagation of near-inertial, internal waves down into deep layers of the ocean is one of the major mechanisms by which wind energy is transported to the oscillations of the ocean in the spectrum range of internal waves. The estimates of Alford (2001) indicate that approximately 0.3 TW of wind power is transferred to the ocean (1 TW = 10^{12} W). The contribution is actually greater because the author considers only the latitudinal band between 50°N and 50°S, excluding the northern and southern higher latitudes with very strong winds. This value is smaller than but comparable to the barotropic tide dissipation rate. Nilsson (1995) estimates the power input on a global scale from hurricanes only to near-inertial waves as 0.01 TW.

Strong atmospheric forcing at the ocean surface caused by fast propagation of hurricanes is a generator of strong inertial oscillations. High values of shear appearing due to strong winds (Sanford *et al*., 1987) generate internal waves at a frequency close to inertial since inertial oscillations are natural oscillations of the ocean. The shear generates internal waves with near-inertial frequencies (as the Richardson number becomes sub-critical). Near-inertial wave motion also occurs due to convergences and divergences in the motion induced by wind in the upper layer (Alford, 2001). After generation at the surface, inertial oscillations slowly spread downwards in the water column as internal waves with a frequency close to inertial. In the vertical (z)–horizontal (x) plane the trajectory of inertial perturbations propagating downwards will differ only slightly from the horizontal since the angle of propagation is determined by the relationship

$$\frac{dz}{dx} = \pm\left(\frac{\omega^2 - f^2}{N^2 - \omega^2}\right)^{1/2}, \qquad (1)$$

where ω is the wave frequency close to the inertial frequency f, and N is the Brunt-Väisälä frequency.

The frequency of wind-generated, near-inertial, internal waves ω is slightly greater than the local inertial frequency f. The inclination of the vector of group velocity to the horizontal for inertial oscillations is much smaller than that of the internal tides. The inclination of group velocity for internal tides is of the order of 1/10 (half wavelength, 50 km, divided by the ocean depth, 5 km; thus the rate of vertical energy spreading for internal tides is of the order of 1000 m per hour). Depending on the difference between the effective frequency of near-inertial oscillations and the local Coriolis parameter, the inclination can range from 10 to 100 times smaller. Thus, a typical inclination of the group velocity of near-inertial waves to the horizontal can vary from 0.01 to 0.001. Accordingly, the place where near-inertial waves reach the bottom should be located at a distance of at least one or a few hundred kilometers from the place where they were generated. Thus, it is unlikely that near-inertial, internal waves can form vertical modes. Speaking about their vertical wavelength we should keep in mind that this is their vertical scale.

The approach adopted in this study is to trace the beams of inertial oscillations propagating downwards. The vertical normal mode approach is hardly applicable here because decomposition of beams into combinations of modes requires many measurements in the vertical, and thus a greater number of levels of observation is required than those at present available from our measurements (only one level of observations in the upper layer and only four or five in the vertical).

Dominating downward propagation is related to this band. The spectrum of downward propagating, near-inertial, internal waves are more energetic and broader than that of upward propagating waves. It is noticeable hat downward propagating waves have lower frequency that the upward propagating waves (D'Asaro and Perkins, 1984).

The normal mode approach has been applied in several papers studying the response of the upper ocean to hurricanes, which has been studied in many papers. Price (1981) analyzed the propagation of hurricanes over moorings and introduced a numerical model to simulate the processes in the upper ocean. Entrainment is the main mechanism that decreases the surface temperature below the hurricane, depending on the hurricane strength and translation speed as well as on the initial depth of the mixed layer and temperature gradient in the thermocline. The response depends only slightly on latitude and hurri-

cane size.

Mao *et al*. (2000) applied a numerical model to study the response of the upper layer of the ocean to tropical cyclones and the dependence of intensification of passing cyclones on the parameters of the warm mixed layer. The rate of intensification and final intensity of tropical cyclones are sensitive to the depth of the mixed layer, but their tracks and gross features are practically unaltered.

The response of the ocean to moving storms is divided into two stages, the first of which is the passage of the storm and generation of currents in the surface layer, while the second stage, after the forcing has ceased, is the adjustment of the ocean towards equilibrium in the wake of the storm (Gill, 1984; Garrett, 2001). Price *et al*. (1994) dealt with the response of the upper layer of the ocean to hurricanes. These authors analyzed the measurements obtained by air-deployed expendable current profilers (AXCP) and applied a numerical model. The forced response includes generation of surface currents and cooling of the surface. The timescale of forced stage response is typically half-a-day. The adjustment stage of the response is baroclinic. The energy of wind-driven currents in the mixed layer is dispersed in a spreading wake of near-inertial, internal waves that spread into the thermocline.

Downward propagation of near-inertial waves generated by storms was studied by Qi *et al*. (1995) based on densely located current meters on moorings in the upper layer. The generation of waves in the mixed layer was followed by their gradual propagation into the thermocline, which lasted for many days after the storm.

Near-inertial waves generated by a hurricane would spread following the direction of the hurricane propagation. The northward propagation of near-inertial, internal waves can be limited by the fact that the northern latitudes can become critical, in the sense of internal wave existence, to the wave generated at southern points with frequencies very close to the local inertial frequency.

Here we consider that the propagation of near-inertial waves generated by a fast moving hurricane is similar to the following physical processes: (1) propagation of ship waves when the velocity of the ship is greater than the speed of surface waves (a bow bore for very fast boats with a supercritical local Froude number, $Fr = V_{\text{ship speed}}/C_{\text{surface wave velocity}}$); (2) propagation of sonic shock wavefront after a supersonic airplane (or bullet). This is described by the Mach cone, whose angle of inclination is related to the Mach number, $M = V_{\text{airplane}}/C_{\text{sound velocity}}$; (3) propagation of Cerenkov electromagnetic radiation emitted by a charged particle moving in an insulating medium at a speed greater than the speed of light in that medium, causing the blue glow tail wake. In the case of near-inertial, internal wave propagation after a hurricane, a dimensionless number similar to the Mach number can be written as $G = V_{\text{hurricane speed}}/C_{\text{speed of near-inertial waves}}$. The hurricane speed (not the wind speed in hurricanes) is usually 10–20 knots, which is 5–10 m/s. The horizontal group velocity of internal waves does not exceed 3 m/s, while the vertical group velocity is in the range 1–10 m/h.

In this paper we analyze the deep ocean response to passing hurricanes as generators of near-inertial, internal waves. We analyze data collected in the northwestern parts of the Pacific and Atlantic oceans in the hurricane season to study the deep ocean response to strong atmospheric forcing. A large number of moorings (more than 100) in the northwestern Pacific allowed us to study the spatial variations in the oceanic response to typhoons and variable downward velocity of near-inertial wave propagation. For a discussion of related methodologies used for internal waves in Straits see (Morozov *et al*., 2002, 2003).

The remainder of the paper is organized as follows. Section 2 is devoted to a succinct description, including shortcomings of the experiments we consider. In Section 3 we comment on the methodologies used for data analysis. The spectrum and bandwidth of data are discussed in Section 4. In Section 5 the fine structure of the spectrum is approximated using a suitable Airy function. Section 6 deals with the downward wave propagation. In Section 7 we discuss the role of vorticity and stratification on the wave velocity. In Section 8 we study the frequency variations due to local vorticity. Finally, in Section 9 we provide a few concluding remarks.

2. Data Description

We consider data from three experiments: *Megapolygon* in the northwestern Pacific in 1987, *Emperor Seamounts* in the northwestern Pacific in 1982, and *Local Dynamics Experiment* (*LDE*) in the northwestern Atlantic in 1978. During each of these experiments, the moorings with current meters deployed in the ocean recorded currents while hurricanes passed through the region.

i) During the *Megapolygon* experiment, 173 moorings with current meters at four depths were deployed in the northwestern Pacific. The study region was located in the Pacific Subarctic Frontal zone. The experiment was carried out during August–October, 1987. The moorings were located within a rectangle with boundaries 38°05.0′ N, 42°29.5′ N, 151°32.0′ E, 157°36.0′ E centered at 40°N, 155°E. They were deployed on a triangular grid with 23 nautical miles spatial separation. Such a large ocean region with dense location of moorings made it possible to study the spatial variability of near-inertial, internal waves. The bottom depths ranged between 5200 and 5800 m and the topography was relatively smooth. The moorings were deployed from three vessels. It started from the west on July 31, and all the moorings were deployed

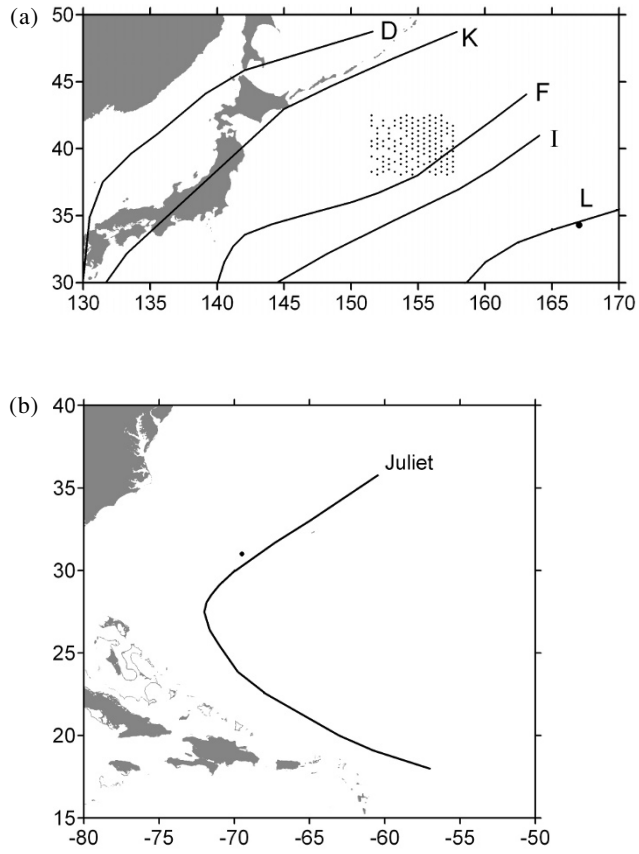

Fig. 1. (a) *Megapolygon* study region and tracks of typhoons in 1987: *Dinah* (D), *Kelly* (K), *Freda* (F), and *Ian* (I). Dotted region gives the locations of moorings. The track of the tropical cyclone *Lola* in September 1982 is indicated as L and the location of mooring 101 on the track of *Lola* is shown with a larger black dot near the lower right corner of the figure (abscissa: longitude, E; ordinate: latitude, N). (b) Region of the *Atlantic LDE* and track (solid line) of hurricane *Juliet* in 1978. Location of mooring 640 on the track of *Juliet* is shown with a black dot (near the solid line) (abscissa: longitude, W; ordinate: latitude, N).

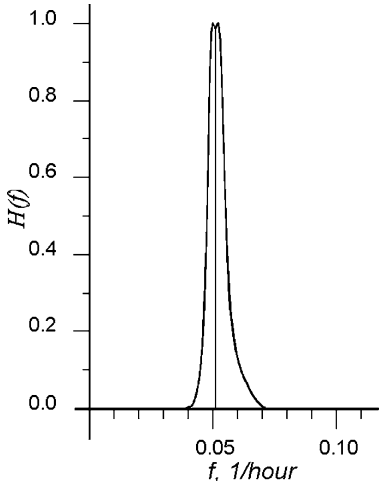

Fig. 2. Frequency response function of the four-pole, bandpass elliptic filter tuned to f = 1/19.5 cyc/hours.

by August 23. Recovery started on October 6, and the experiment ended on October 24. During the period of operation some buoys were displaced, drifted, or lost due to strong currents, storms, and ongoing fishing activity in the region. These losses required permanent replacement by new moorings. All moorings were equipped with vector-averaging current meters, type "Potok", with temperature sensors (Maximenko *et al*., 2001; Lozovatsky *et al*., 2003). The instruments were set at 120 and 1200 m depths. Some of the moorings were also equipped with instruments at 400 m and 4500 m. The averaging time and sampling interval was 30 min. Unfortunately, instruments were lost and damaged, and some data were lost due to malfunctioning of the meters, even on recovered moorings. The losses are estimated as 50%. However, the experiment allowed dense coverage of the study region with significant time series of measurements.

During the operation of the moorings, several typhoons passed over the study region. The following typhoons had the strongest influence: *Dinah*, which passed north of the study region on August 31–September 1; *Holly*, which passed southeast of the region on September 17; *Freda* (the strongest of them all), which crossed the southeastern part of the region from southwest to northeast on September 17–18 (the maximum wind speed was 50 m/s and lowest pressure reached 976 mbar); *Ian*, which passed the southeastern edge of the region on October 3, and finally, *Kelly*, which passed north of the region on October 18.

ii) The *Emperor Seamounts* experiment in 1982 was conducted in the northwestern Pacific (WOCE data disk, mooring B CMDB accession numbers 101 and 102 for levels 425 and 1125 m, respectively). The measurements were made with Aandera RCM5 meters. The mooring was located at 34°20′ N, 167°02′ E. Typhoon *Lola* passed through the location of the mooring on September 19, 1982.

A chart of the northwestern Pacific region with locations of moorings and tracks of the strongest typhoons is shown in Fig. 1(a).

iii) The *Atlantic LDE* was carried out in 1978 and data are readily available (WOCE data disk, mooring WHOI 640, CMDB accession numbers 1119, 1118, 1133, 1137, 1123, for levels 269, 394, 516, 839, and 2008 m, respectively). The mooring was located at 31°01′ N, 69°30′ W. Hurricane *Juliet* passed the point of the mooring on October 10, 1978. A chart of the region with the mooring location and the track of hurricane *Juliet* is shown in Fig. 1(b).

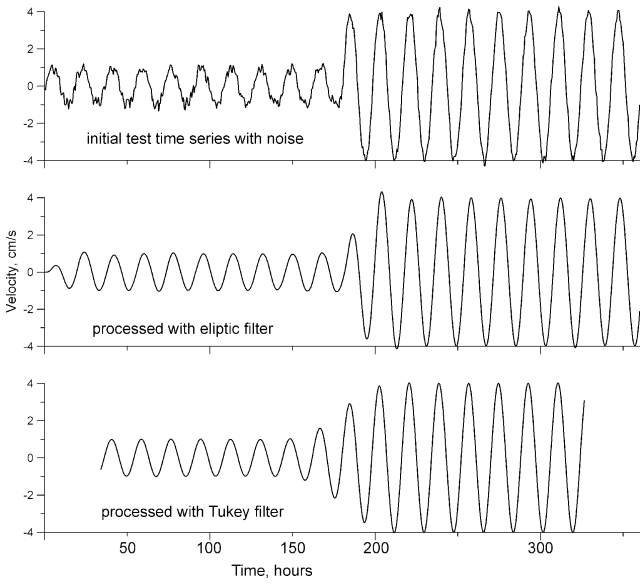

Fig. 3. Example of processing a time series using the four-pole, band-pass elliptic filter and Tukey filter. The initial sinusoidal test series with noise is shown in the upper pattern. The processed time series after band-passing are shown in the lower patterns.

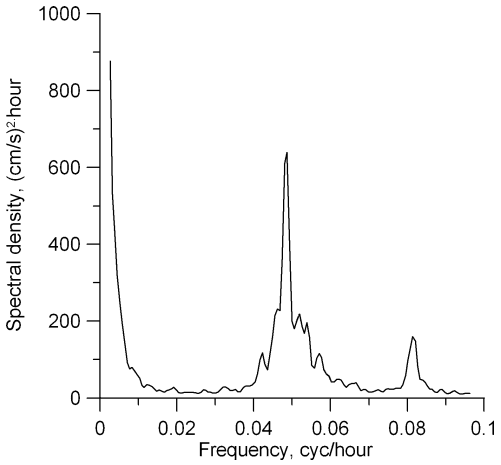

Fig. 4. Typical frequency spectrum of velocity calculated from 409-day measurements close to *Emperor Seamounts* in the Pacific at 425 m depth (mooring 101).

3. Data Analysis Methodologies

The analysis of inertial components of the velocity time series measured at moored buoys was performed after band-pass filtering to demodulate the near-inertial signal. The initial time series were sampled with a time interval of 30 min. The inertial period in the *Megapolygon* study region ranges from 17.9 to 19.5 h.

The matlab programming software was used to band filter the time series, applying the 4-pole 40 dB elliptic band-pass filter (Parks and Burrus, 1987). In the *Megapolygon* region the filter was tuned to a central frequency of 1/19.0 h^{-1} with the high-low frequency cutoffs at 1/17 h^{-1} and 1/20.5 h^{-1}, respectively. The frequency response function $H(f)$ of this filter is shown in Fig. 2. In the study regions of the *Emperor Seamounts* and *LDE* the filters were similarly tuned to a frequency slightly (1.05) greater than the corresponding local inertial frequency.

An example of time series processing using a test record consisting of an 18.0-hour period sinusoidal test oscillation of unit amplitude with noise, which sharply increases by a factor of four in the middle of the time series, is shown in Fig. 3. A sharp jump in the amplitude modulates the passage of a near-inertial oscillation with increased amplitude. The elliptic filter produces a very low amplitude distortion and phase shift after the sharp increase in the amplitude.

We also used the Tukey band filter tuned to the same frequency band (Blackman and Tukey, 1958). The results of processing using these two methods of filtration differ in detail, but the general features are the same. The results of processing the test time series are shown in Fig. 3 (see below Figs. 11 and 12).

4. Spectrum and Bandwidth of Available Data

We begin our analysis with a description of spectra in the inertial band. The near-inertial interval of the spectrum dominates over the remaining part of the spectrum (we do not analyze very low frequencies here). The spectrum therefore is steeper at the high frequency border of the inertial band. A typical frequency spectrum of velocity is shown in Fig. 4. It is a spectrum calculated from 409-day measurements close to the *Emperor Seamounts* in the Pacific at a depth of 425 m.

The spectral densities in the inertial band are non-uniformly distributed over the square of the study region, depending on the local peculiarities of generation and mean state of the ocean, which influences the ocean, response to wind forcing. This is clearly seen in the *Megapolygon* study region. Contour lines of spectral densities at the inertial peak at 1200 m are shown in Fig. 5 over the background of the chart of the *Megapolygon* with contour lines of temperature at 300 m, showing the dynamic structure in the region. Numbers on contour lines indicate isotherms. Note an anticyclonic warm eddy centered at 40°N, 153°E. Note also the general feature of increasing values in the region of the anticyclonic mesoscale eddy location and close to the boundary with the Kuroshio Current in the south, which can be explained by the transfer of the eddy and current energy to the inertial band and by trapping of near-inertial waves in the regions of anticyclonic vorticity. The background iso-

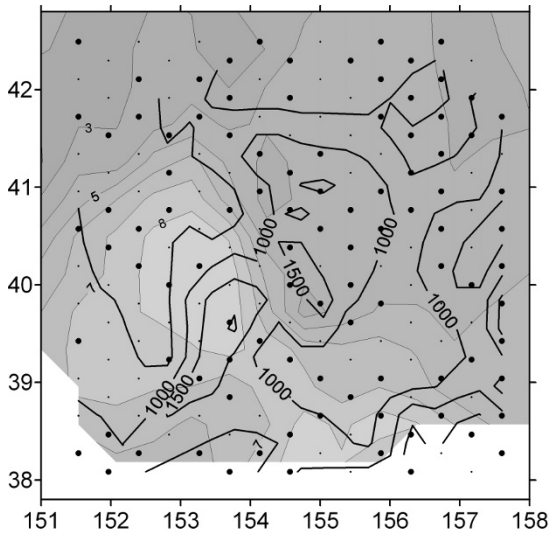

Fig. 5. Contour (thick solid) lines of spectral densities at the inertial peak at 1200 m [(cm/s)^2·h] are shown over the background of the chart of the *Megapolygon* with contour lines of temperature at 300 m (thin lines, grayscale) showing the dynamic structure in the region. Large numbers are related to thick solid contour lines of spectral density. Small numbers beside thin solid contour lines of temperature indicate isotherms. An anticyclonic warm eddy is centered at 40°N, 153°E. Small dots show planned locations of moorings. Large dots show moorings with data (abscissa: longitude, E; ordinate: latitude, N).

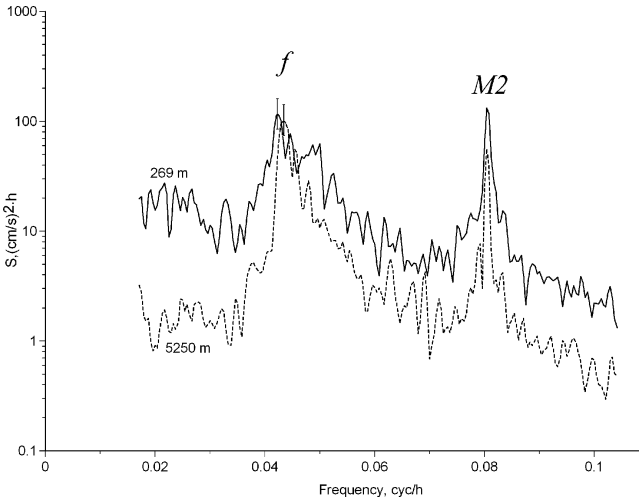

Fig. 6. Velocity spectra of the *LDE* experiment at 269 m and 5250 m. Confidence limits (95%) are shown at the inertial peaks.

therm chart was plotted on the basis of hydrographic survey data obtained in August of the same year as the experiment. The moored data for the spectral analysis were accumulated from August to the beginning of October. By the end of the experiment the anticyclonic eddy was displaced to the east. Thus, increased spectral densities near 155°E can be related to the displacement of the eddy. Another feature of the distribution is a general trend of increase from north to south and from west to east. We attribute the latter to the influence of two hurricanes (*Freda* and *Ian*), which passed in the southeastern part of the region.

In the time series measured in the deep layers the inertial peak on the spectra is displaced to higher frequencies. Only near-inertial waves with a frequency greater than the local inertial frequency being generated at the surface can propagate to the depths and reflect from the bottom. When the waves reach the bottom the difference by which the wave frequency exceeds the local inertial period can be considered as a measure of the width of the near-inertial band within which the energy propagates downward (Garrett, 2001). We show two spectra for the measurements during the *Atlantic LDE* in 1978–1979 (446 days long). One time series was measured at 269 m and the other at 5250 m, which was 100 m above the bottom. The spectra are shown in Fig. 6; the vertical axis has a logarithmic scale. The local inertial period is 0.0429 cyc/h. A sharp decrease in the spectral density occurs at 0.0570 cyc/h, which is approximately 1.25*f*. A notable shift of the peak is observed for deep time series. The peak at 269 m corresponds to a frequency of 0.425 cyc/h, while the corresponding peak at 5250 m is shifted to frequency 0.433 cyc/h. This does not occur with the M2 peak at different depths. Thus, the effective Coriolis parameter is decreased by vorticity. Only the high frequency part of the oscillations in the inertial band propagates to the bottom, as shown on the graph. The inertial bandwidth in the regions influenced by hurricanes is generally wider than in regions, where hurricanes are not observed. It is our opinion that the wider peak is caused by near-inertial, internal waves propagating from distant northern latitudes after strong generation by hurricanes.

5. Fine Structure of the Spectra in the Inertial Band (Airy Function Approach)

Theoretical models of inertial oscillations in terms of free wave packets at the turning points were developed by Munk and Phillips (1968) and Munk (1980). The equation obtained for the amplitudes of inertial oscillations of velocity in the neighborhood of the local inertial frequency φ_0 is the Airy equation (Abramowitz and Stegun, 1972):

$$\frac{d^2V}{d\eta^2} - \eta V = 0, \qquad (2)$$

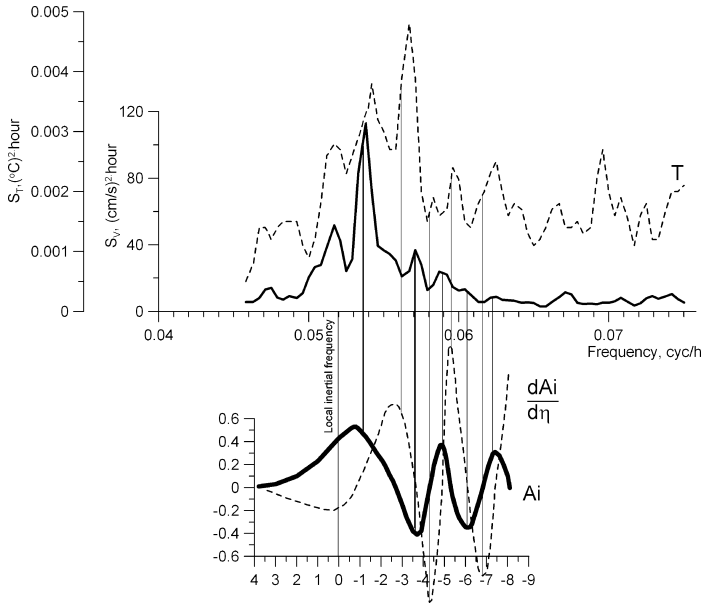

Fig. 7. Upper figure: Inertial band of velocity (V) and temperature (T) spectra (upper panel). Lower figure: Airy function (Ai) and its derivative (dAi/dη) are shown in the lower part of the figure with the abscissa and ordinate corresponding to the argument of the Airy function. Measurements were made at mooring 104 of the *Emperor Seamounts* experiment at 940 m (38°58′ N, 171°06′ E). Spectral maxima are connected to extrema of the Airy function and its derivative.

where $\eta = (\varphi - \varphi_0)/L + (\alpha L)^2 - (\sigma - 2\sin\varphi_0)/2L\cos\varphi_0$ is the Airy argument; $L = (\gamma^2 \sin 2\varphi_0)^{1/3}$ defines the Airy scale, $\gamma = \sqrt{10^5 r}$, $r = 1, 2, \ldots$; $\alpha = s/\cos\varphi_0$ is the local wavenumber, $\sigma = \omega/\Omega$ is the dimensionless frequency, $\sigma_0 = 2\sin\varphi_0$ is the dimensionless inertial frequency, φ_0 is the initial latitude, φ denotes the local latitude, and r is the vertical mode number.

The solutions of the Airy equation are written as Airy functions, *Ai*, of argument η. They describe a displacement of the inertial peak to higher latitudes relative to the local inertial frequency and sawtooth structure of the inertial peak.

The vertical group velocity of internal waves decreases to zero as the frequency of the wave becomes equal to the local inertial frequency. Thus, waves with frequencies greater than the local inertial frequency can propagate downwards from the surface of the ocean since the generation of inertial oscillations occurs mainly at the ocean surface.

In measurements of currents with moored instruments located at different depths, the inertial peak is always displaced to greater frequencies for measurements in very deep layers (~4000 m). Only the oscillations with frequencies higher than the local inertial frequencies can reach deep layers of the ocean. It is likely that an exception to this consideration is the generation of inertial oscillations at great depths caused, for example, by a hydraulic pressure jump and ocean level fluctuations (up to 20 cm) (Shay *et al*., 1990) when a hurricane passes over the region. According to different models (Pollard, 1970; Fu, 1981), inertial oscillations can be generated either by a pressure change or by wind forcing.

The spectral peak at the inertial frequency is characterized by the fine structure described by the Munk-Phillips model. In particular, the spectrum of horizontal velocity, S_u, is proportional to the squared Airy function,

$$S_u \sim \left[Ai(\eta)\right]^2, \tag{3}$$

while the vertical velocity, and consequently buoyancy and temperature spectra, S_T, are proportional to

$$S_T \sim \left[\frac{dAi(\eta)}{d\eta}\right]^2. \tag{4}$$

Munk and Phillips (1968) considered that experimental verification of the theoretical form of the spectrum requires a resolution of 0.005 cycles per day, which requires a duration of the time series equal to 1000 days (approximately 3 years). The duration of measurements at the *Emperor Seamounts* experiment was slightly greater than one year and we could provide a resolution of only 0.01 cycles per day.

The spectra of horizontal velocity and temperature measured at mooring 104 of the *Emperor Seamounts* ex-

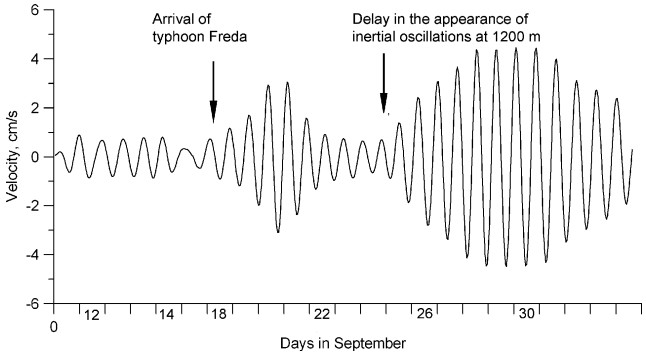

Fig. 8. Time series of velocity after band filtering from mooring 1118 (39°26′ N, 151°32′ E). A packet of near-inertial waves appeared on September 18 due to a pressure jump caused by the propagating typhoon. Later, wind generated, near-inertial oscillations spread downwards, propagating to a depth of 1200 m (September 25).

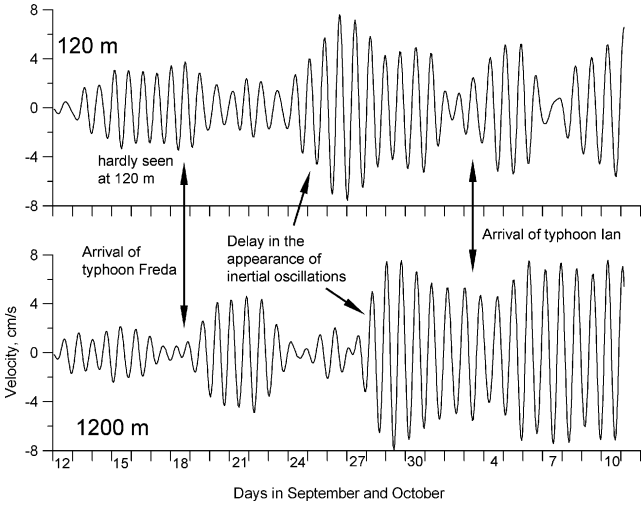

Fig. 9. Time series of velocity after band filtering. Mooring 1814 (40°46′ N, 154°34′ E). A near-inertial wave packet was generated at 1200 m on September 18 by a pressure jump caused by the typhoon's propagation. A similar event is barely noticeable at 120 m. Later, wind-generated, near-inertial oscillations spread downwards and propagated to 120 m depth on September 22 and even to 1200 m on September 28.

periment at 940 m depth are shown in Fig. 7. The inertial bands of the spectra are compared with the Airy functions approximation.

The Airy function and its derivative are shown in the lower part of Fig. 7. The parameter value $r = 3$ selected for the Airy function gives the best fit to the spectra approximation. For clarity, the peaks of the spectra of velocity are connected with vertical lines to the maxima and minima of the Airy function (thick solid line) shown in the lower part of the figure since the spectrum is proportional to the square of the Airy function. The maximum of the velocity spectrum is displaced to higher frequencies by approximately 0.05 of the local inertial frequency. The maximum of the Airy function corresponds to the value of the Airy argument equal to minus 0.8. In similar manner the maxima of the temperature spectra (broken line) are connected with vertical lines to the minima and maxima of the derivative of the Airy function (broken line). The local inertia frequency is superimposed at the value corresponding to the zero of the Airy argument.

6. Downward Propagation of Near-Inertial, Internal Waves

We now analyze the downward propagation of near-inertial, internal waves on the basis of the data provided by the moored measurements in the *Megapolygon*, *Emperor Seamounts*, and *Local Dynamic Experiments*.

Typhoon *Freda* passed through the *Megapolygon* study region on September 18, 1987 with a translation velocity of 18 knots (36 m/s) and maximum wind velocity of 60 knots (30 m/s). The eye of the typhoon passed the moorings considered below at different distances, reaching out to 100–150 km. The moorings were located

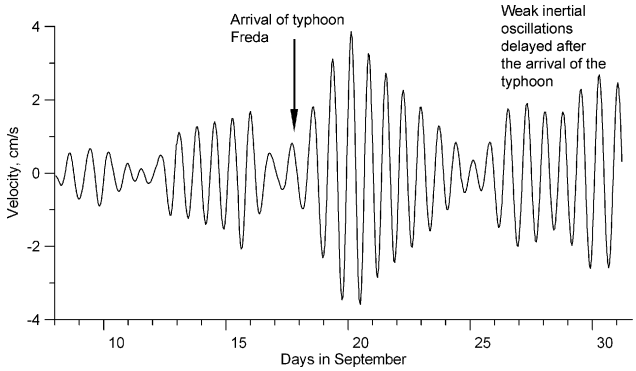

Fig. 10. Time series of velocity after band filtering from mooring 2211 located at 42°06′ N, 156°18′ E. A near-inertial wave packet was generated at 1200 m on September 18 by a pressure jump caused by the typhoon's propagation. Later, weak, wind-generated, near-inertial oscillations spread downwards and propagated to 1200 m (September 26).

in the zone where winds change their direction from southwest to south and then to southeast.

For the analysis we tune the central frequency of the band filter to a frequency approximately 5% greater than the local inertial frequency, assuming that the inertial peak is best approximated by the Airy functions.

The current measurements at moorings 1118, 1512, 1814, 2211 (shown below in Figs. 8–12) and other moor-

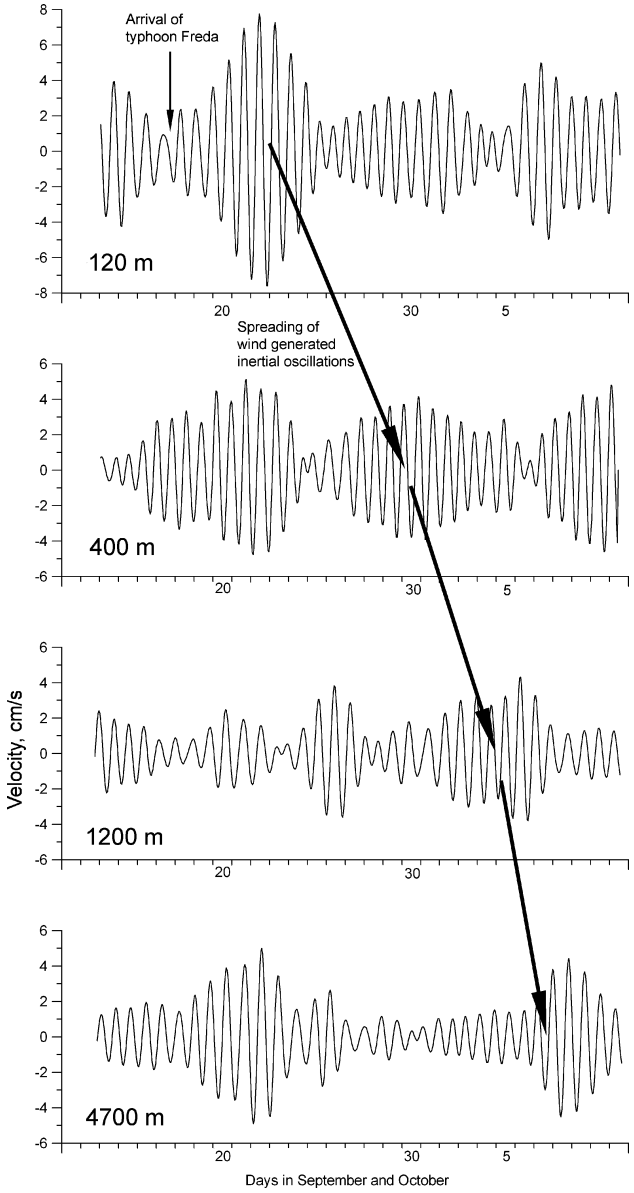

Fig. 11. Time series of velocity after band filtering using the four-pole band-pass elliptic filter showing downward propagation on a near-inertial wave packet. Data from mooring 1512 (41°43′ N, 153°16′ E).

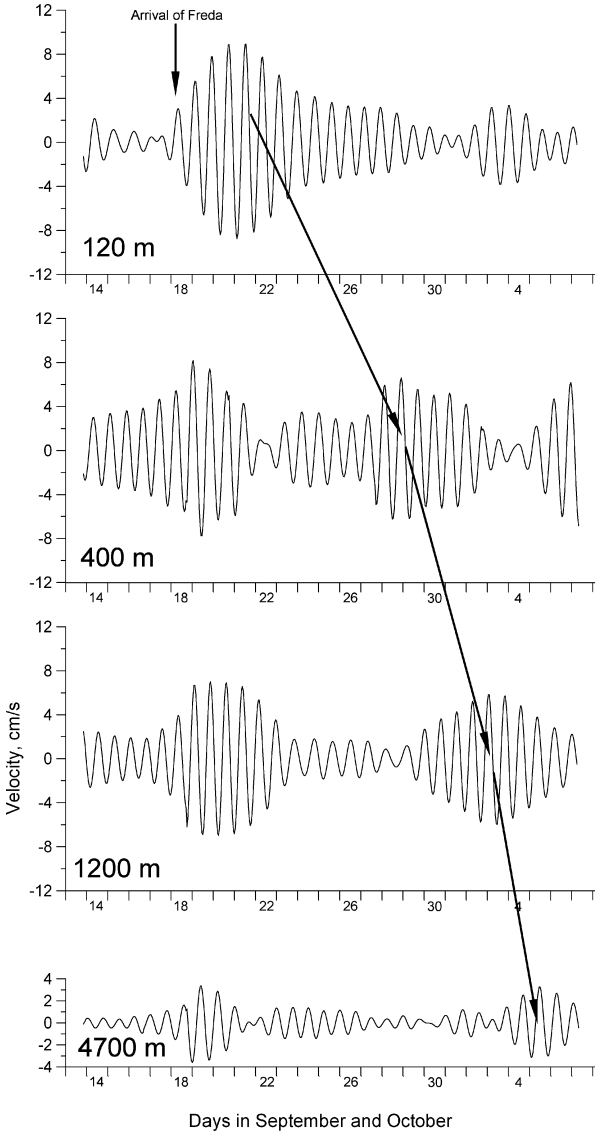

Fig. 12. Time series of velocity after band filtering using the Tukey band-pass filter showing the downward propagation on a near-inertial wave packet. Data from mooring 1512 (41°43′ N, 153°16′ E).

ings indicate that strong near-inertial oscillations were generated almost immediately after the passage of the typhoon at all depths down to 1200 m. A similar response was reported in (Shay and Elsberry, 1987). The current vectors rotated clockwise with amplitudes ranging from 6 to 10 cm/s. Another wave packet of near-inertial waves was recorded after a few days. We interpret the initial oscillations generated on September 18 as those caused by a pressure jump and sharp variations in the ocean level associated with the typhoon's propagation. These near-inertial waves were generated simultaneously at all levels. The second wave packet was generated by wind forcing at the surface and propagated slowly downwards, reaching 1200 m on September 25 and even later at different moorings.

The velocity time series after band filtering at mooring 1118 (39°26′ N, 151°32′ E) is shown in Fig. 8. A near-inertial wave packet was generated on September 18 by a pressure jump caused by the typhoon's propagation. Later, wind-generated, near-inertial oscillations spread downwards, propagating to a depth of 1200 m on September 25.

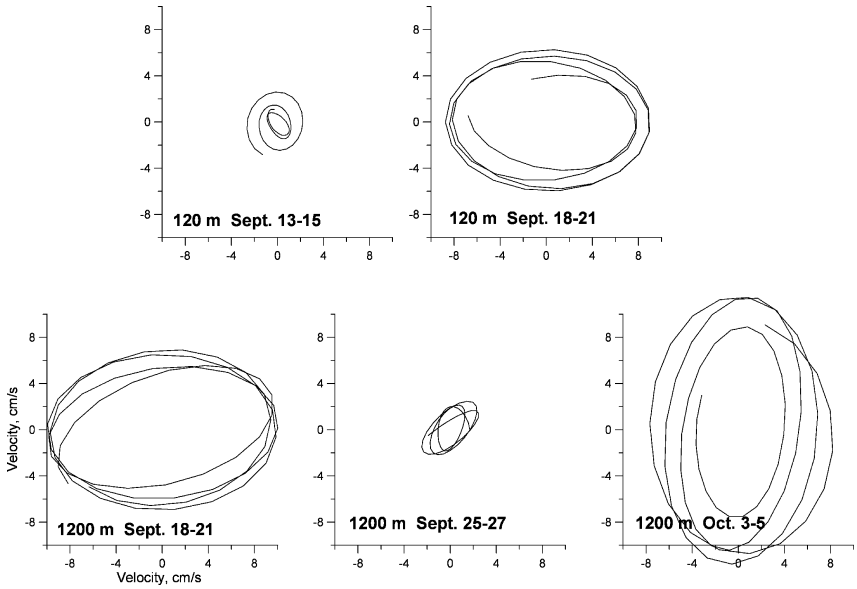

Fig. 13. Trajectories of the velocity vector (hodographs) measured at mooring 1512 (41°43′ N, 153°16′ E) at 120 and 1200 m: (a) 120 m, September 13–15, before arrival of typhoon *Freda*; (b) 120 m, September 18–21, arrival of typhoon *Freda*; (c) 1200 m, September 18–21, arrival of typhoon *Freda*; (d) 1200 m, inertial oscillations decayed after arrival of typhoon *Freda*; (e) wave packet generated by typhoon *Freda* at the surface reached 1200 m on October 3.

Velocity time series at mooring 1814 (40°46′ N, 154°34′ E), after band filtering, are shown in Fig. 9. A near-inertial wave packet is generated at 1200 m on September 18 by a pressure jump caused by the typhoon's propagation. A similar event is almost unnoticeable at 120 m. Later, wind-generated, near-inertial oscillations spread downwards, propagating to depths of 120 m on September 22 and later, on September 28, down to 1200 m. Since the angle of the inclination of group velocity of near-inertial, internal waves is small, the wave packet recorded at 1200 could be generated by the hurricane at a rather large distance from the mooring. The direct influence of the hurricane at 120 m is not well seen since the hurricane was passing the region with a translation velocity of 18 knots (9 m/s), so the direction of the winds changed rapidly. Thus, near-inertial waves generated by the wind in the northern sector of the typhoon could be suppressed by the waves generated in the southern sector.

The generation of inertial oscillations is very sensitive to variations in wind speed and direction, and they cannot be predicted in the absence of local wind records (Pollard, 1980). The generation of near-inertial, internal waves by wind is enhanced if the direction of the wind remains constant during a sufficiently long time interval (Pollard, 1970). According to Treguier and Klein (1994), inertial oscillations propagating against the wind extract energy and become amplified. Kundu (1984) analyzed the response of inertial oscillations to rapidly variable wind. The root mean square (r.m.s.) response initially increases with time as $t^{1/2}$, until the stationary state is reached. Continuous random forcing preferentially increases subsurface amplitudes, since the energy flux from the surface causes a surface decay and a subsurface growth of the response.

Since hurricanes propagate very rapidly, the wind direction over a specific point can change to the opposite on the day the hurricane arrives, so strong generation in the upper layer may not occur. A clearly manifested wave packet of inertial oscillations at greater depths could propagate from wind generated waves arising remotely from the region where the change of the wind direction was not abrupt. Maeda *et al*. (1996) found that inertial oscillations are effectively generated at the eastern margin of a typhoon during the rapid decrease of wind velocity, rather than by a prevailing strong wind.

Figure 10 shows velocity time series at mooring 2211 located at 42°06′ N, 156°18′ E, after band filtering. A packet of near-inertial waves is generated at 1200 m on September 18 by a pressure jump caused by the typhoon's propagation. Very often inertial oscillations, even at deep levels, start a few hours before the typhoon's arrival. This was noted in (Shay and Elsberry, 1987). Generation of near-inertial waves before the direct forcing by a typhoon can be explained by the existence of pressure perturbation in a larger region induced by a moving typhoon. Later, near-inertial oscillations generated by wind spread downwards propagating down to 1200 m on September 26.

Below we show the time series processed by the el-

liptic filter and Tukey filter at mooring 1512 located at 41°43′ N, 153°16′ E. The band filtering results using the elliptic filter are shown in Fig. 11 and the results obtained using the Tukey filter are shown in Fig. 12. Both filters demonstrate the general downward propagation of near-inertial oscillations, but differ in detail.

The inertial oscillations generated by a hurricane last up to 10–12 days after which they reach the background level or else a new wave packet arrives. However, some publications report a longer lifetime of inertial oscillations (18–20 days) (Brink, 1989; Taira *et al.*, 1993).

After generation of the wave packet on August 18, the perturbations reached a depth of 400 m on August 27. The vertical velocity is estimated as 2.5 m/h. The packet appeared at 1200 m on August 29. The vertical velocity increased due to weaker stratification in the deeper layers and we estimate it as 16 m/hour. During another five days, the wave packet propagated down to 4700 m with a velocity of 30 m/hour. The Brunt-Väisälä frequency at great depths becomes as small as $0.3 \cdot 10^{-2}$ s^{-1}, which is approximately 10 times smaller than in the upper layer. Thus, an almost ten-fold increase in the vertical velocity is not surprising.

The forms of trajectories of velocity vectors (hodographs) add more information to the downward propagation of near-inertial waves. Hodographs of the velocity vector at 120 and 1200 m based on the measurements at mooring 1512 located at 41°43′ N, 153°16′ E, are shown in Fig. 13 for different time periods relative to the typhoon's arrival. Before the typhoon *Freda*'s arrival on September 18, the hodographs at 120 m are almost circles and the velocities are small. Beginning from the day of the typhoon's arrival, the amplitude of hodographs increases and they become elliptical. The latitudinal constraint does not allow the velocity vector to increase much in the north-south direction compared to the west-east direction. Since the frequencies of the generated oscillations are close to inertial, they cannot propagate northward following the path of the typhoon. In the course of its northward travel the typhoon generates inertial oscillations with increasingly higher frequencies. Down at the 1200 m level we see similar generation immediately after the typhoon's passage. The hodographs are elongated in the east-west direction. The near-inertial oscillations generated by the pressure jump associated with the passage of the typhoon decay in a few days (September 25–27). On October 3, when the near-inertial wave packet generated earlier at the surface by wind forcing reaches the 1200 m level the hodographs of the velocity vector become elliptical and are elongated in the north-south direction, which presumably indicates that the waves were generated north of the mooring location and propagated in the southerly direction.

One more confirmation of the penetration of near-

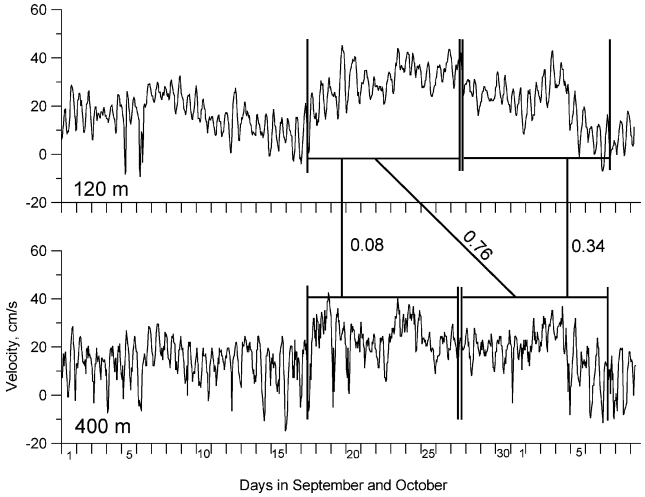

Fig. 14. Time series of current measurements from mooring 1512 at 120 and 400 m. Straight vertical lines delineate the time intervals for calculating coherences in inertial frequency. Coherences between simultaneous time series are low (0.08 and 0.34). The coherence between time series with a time shift corresponding to the times of the wave-packet of near-inertial waves arrival increases up to 0.76. See Figs. 11 and 12 to view the demodulated inertial oscillations during the same time interval.

inertial waves downwards is obtained by estimating the coherence of initial time series between different levels of measurements with a time shift. The example below demonstrates the coherences calculated between velocities measured at 120 and 400 m on mooring 1512. If analyzed both time series starting on September 17, the coherence is low (0.08). It is slightly higher if both time series start on September 27 (0.34), but it does not exceed the 95% confidence level, which is 0.48. If we calculate coherence between time series at 120 m starting on September 17 and at 400 starting on September 27, which corresponds to the times when the wave packets of near-inertial waves appear at 120 and 400 m, the coherence increases significantly to 0.76 (Fig. 14).

The *Emperor Seamounts* experiment was carried out in 1982–1983 east of the *Megapolygon* study region. Typhoon *Lola* passed through the point of the mooring location on September 18, 1982. The typhoon originated on September 13 and four days later it accelerated and propagated rapidly out of the subtropics. Band-filtered inertial oscillations of velocity are shown in Fig. 15. The typhoon's arrival was marked by a low level increase in the amplitudes at a depth of 425 m. Wind generated oscillations propagated downwards and reached the instrument at 425 m five days later on September 23. The subsequent propagation of the wave packet was recorded by the instrument at 1125 m on September 30.

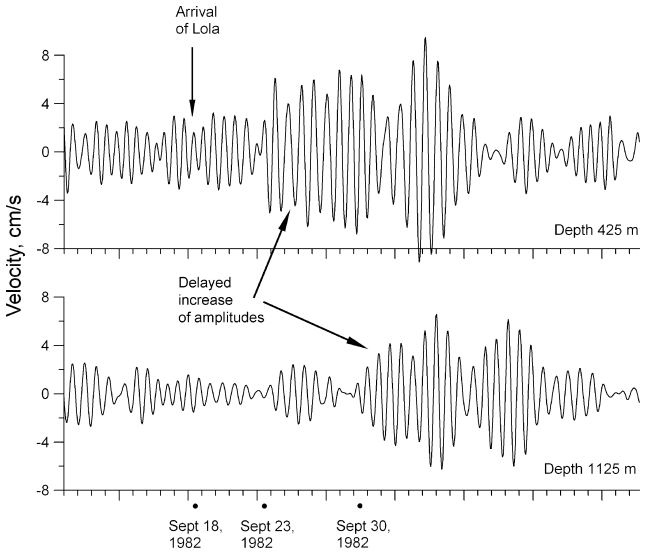

Fig. 15. Depth variation of near-inertial waves generated by typhoon *Lola* close to the *Emperor Seamounts*. The typhoon passed through the mooring on September 18, 1982.

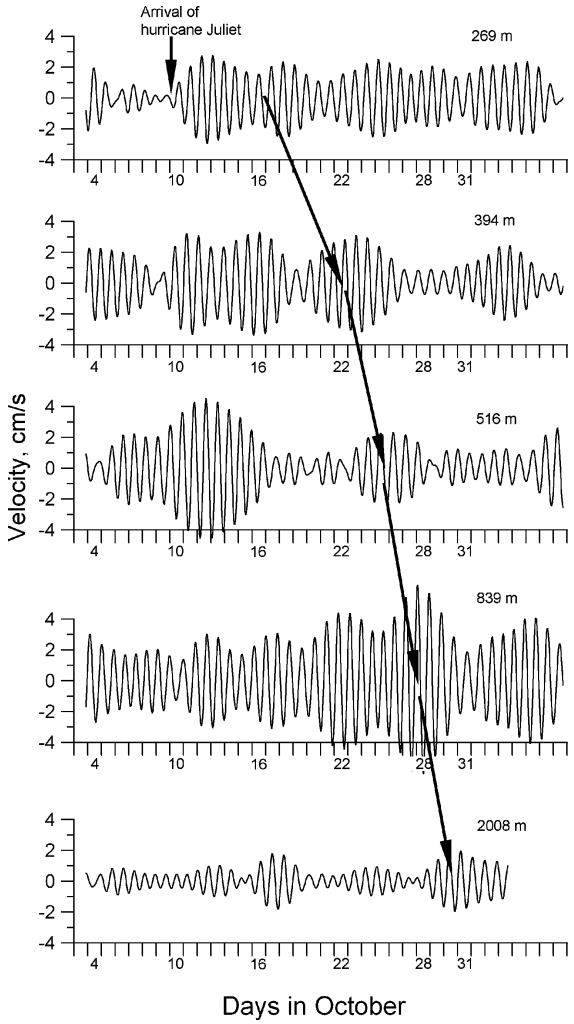

Fig. 16. Depth variation of near-inertial waves generated by hurricane *Juliet*, in the Atlantic (1978). The hurricane passed through the mooring on October 9, 1978.

A similar pattern of downward propagation of near-inertial oscillations was observed in the Atlantic Ocean in 1978 during the *LDE*. Hurricane *Juliet* was formed from a tropical wave on October 7 about 600 miles east of Puerto Rico. The storm passed north of the island, attained a wind speed of 50 mph, and headed into the Sargasso Sea to the region of the *LDE*. Hurricane *Juliet* passed through the mooring point on October 10, 1978. The hurricane faded away on October 11 southwest of Bermuda. Mooring 640 was deployed at 31°01′ N, 69°30′ W. The instruments for measuring currents and temperature were located at depths of 269, 394, 516, 839, and 2008 m. A slight increase in the amplitudes on the day of the hurricane's arrival caused by a pressure jump was observed at all observation depths. Later, the wind-generated, near-inertial waves propagated downwards and reached a depth of 2008 m on October 28 (Fig. 16). Estimates of vertical velocities in different layers show that the vertical velocity of the wave packet increases with depth. The packet reached a depth of 394 m in 10 days, with a mean velocity of 1.6 m/hour. During the following nine days the packet deepened to 2008 m with a mean velocity of 7.5 m/hour, increasing with depth as stratification became weaker.

7. Influence of Vorticity and Stratification on the Speed of Downward Propagation of Inertial Oscillations (*Megapolygon*)

The downward propagation of the energy of near-inertial, internal waves is governed by two main factors: (1) the value of the energy, which is high compared to the energy of higher frequency range; and (2) vertical group velocity, which is low (and tends to zero near f) and extremely variable compared to internal waves of higher frequencies.

We processed all available *Megapolygon* data with the band-filtering procedure and calculated the delay in increase of amplitudes after passage of typhoon *Freda* on August 18. The delay varies within 4–12 days depending on the location of the mooring. The velocity of downward propagation was found to depend on the mean vorticity in the region due to the presence of an anticyclonic eddy and the northern periphery of the Kuroshio Current.

The vertical group velocity of near-inertial waves is given in (Balmforth *et al.*, 1998) $C_g \approx N^2(z)\cdot(k_x^2 + k_y^2)/2f_{eff}k_z^3$. Knowing the relation between k_z and $k^2 = k_x^2 + k_y^2$, which is similar to (1), $N^2(z)$ can be excluded and the group velocity can be approximately written as $C_g \approx$

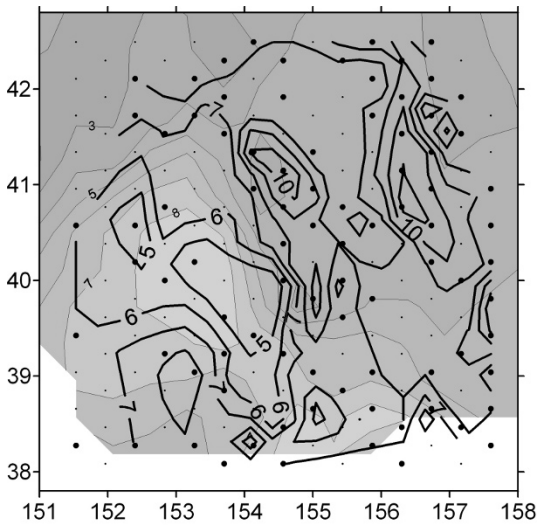

Fig. 17. Delay in the appearance of near-inertial wave packet (in days) at 1200 m after passage of typhoon *Freda*. Numbers by thick solid contour lines indicate time delay. The grayscale chart of the *Megapolygon* with thin solid contour lines of temperature at 300 m shows the dynamic structure in the region. Numbers by thin solid contour lines indicate isotherms. An anticyclonic warm eddy is centered at 40°N, 153°E. Large dots show positions of moorings with data at 1200 m. Smaller, lighter dots indicate locations of lost moorings and hence lost data. Smaller time delays are observed in the northern part and in the region of high clockwise vorticity.

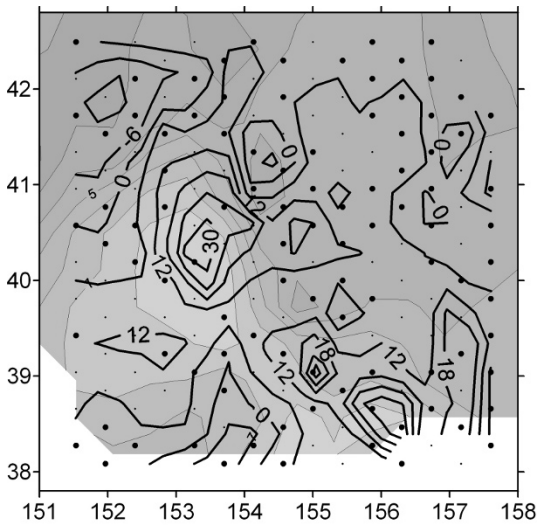

Fig. 18. Deviation of the measured frequency of inertial oscillations from the local inertial frequency over the *Megapolygon* study region. Solid thick contour lines (divided by 10000 to indicate a shift in cycles per hour) show a positive or negative deviation of the measured peak at the inertial frequency from the local inertial frequency. The grayscale temperature chart of the *Megapolygon* with thin solid contour lines of temperature at 300 m shows the dynamic structure in the region. Low numbers by contour lines indicate isotherms. Smaller, lighter dots indicate planned location of moorings at 1200 m. Large dots indicate moorings with data. A slight difference in the number of large dots from Fig. 17 is due to the fact that dots in Fig. 17 correspond only to the data of typhoon *Freda*'s propagation, whereas this figure and Fig. 5 show more data.

$(\omega^2 - f_{eff}^2)/2f_{eff}k_z$. In both relations, the group velocity depends on the components of the wavenumber, which vary with depth and stratification.

In order to analyze the vertical variation in the group velocity it is worth considering the inclination of the vector of group velocity to the horizontal as a function of stratification and vorticity-modified Coriolis parameter. The inclination of the group velocity trajectory relative to the horizontal is determined by the relationship (1). Since the vectors of inertial oscillations and anticyclonic vorticity are in the same direction, the effective frequency of inertial oscillations is increased in the regions of anticyclonic vorticity as $\omega_{eff} = \omega + \xi/2$. The effective local inertial frequency depends on the mean vorticity in the region. The effective inertial frequency is decreased by negative anticyclonic vorticity as $f_{eff} = f_0 - \xi/2$, where f_0 is local inertial frequency and ξ is vorticity. In the regions of negative vorticity (clockwise rotation), the effective inertial frequency decreases. Thus, Eq. (1) becomes

$$\frac{dz}{dx} = \pm\left(\frac{\omega_{eff}^2 - f_{eff}^2}{N^2 - \omega_{eff}^2}\right)^{1/2}, \qquad (5)$$

thus the numerator increases, which leads to an increase in the vertical component of group velocity. A decrease in the effective (vorticity-modified) Coriolis parameter and an increase in the effective frequency of inertial oscillations leads to widening of the inertial band, and hence to trapping of near-inertial waves in this band and their intensification.

The Brunt-Väisälä frequency $N(z)$ in the northern part of the study region is smaller than in the southern one. However, $N(z) >> \omega_{eff}$. Hence, in the northern part of the *Megapolygon* study region the angle of the group velocity is greater than in its southern part. Therefore the time of the near-inertial wave propagation to 1200 m decreases in the northern region.

The delay in the propagation of near-inertial, internal waves to a level of 1200 m related to the time of typhoon *Freda*'s arrival is shown in Fig. 17. Note an anticyclonic warm eddy centered at 40°N, 153°E. Numbers on thick solid contour lines denote time delay (in days) of intensification of inertial oscillations at 1200 m after passage of typhoon *Freda*. Smaller time delays are ob-

served in the northern part, in which stratification is weaker, and in the region of high clockwise vorticity associated with the anticyclonic eddy.

The velocity of downward propagation of energy with the packets of near-inertial waves is estimated as 1–10 m/hour in the depth interval up to 1200 m. In the region of strong currents associated with this eddy, where the vorticity is maximal, downward propagation of energy occurs with a higher speed. This is a manifestation of Taylor columns (Pedlosky, 1987) in the ocean.

8. Variations in the Frequency of Inertial Oscillations Depending on Local Vorticity

Since downward propagation of near-inertial, internal waves depends on mean local vorticity, it is interesting to analyze the spatial distribution of the frequencies of near-inertial waves and their relation to the local mean vorticity. A large number of moorings in the *Megapolygon* region allowed us to study the dependence of the location of the inertial peak on the spectrum on local vorticity, due to the presence of mesoscale cyclonic and anticyclonic eddies and the northern periphery of the Kuroshio Current. As mentioned earlier, the effective frequency of inertial oscillations is influenced by the local vorticity and increases compared to the intrinsic frequency of oscillations as $\omega_{eff} = \omega_{\text{int}} + \xi/2$, where ω_{int} is the intrinsic frequency of inertial oscillations.

Thus, in the regions of anticyclonic eddies the effective frequency of inertial oscillations should increase by 0.5ξ (which is equal to $1.3\cdot10^{-6}$ s^{-1} or $4.7\cdot10^{-3}$ h^{-1}) compared to the intrinsic frequency. A chart showing the shift of the frequency of inertial oscillations over the *Megapolygon* study region is shown in Fig. 18. The values of positive or negative deviation of the measured peak from the local inertial frequency in the figure are in frequency units divided by 10000 to indicate a shift in cycles per hour. The frequency shifts shown by thick solid contour lines vary from $-1.2\cdot10^{-3}$ h^{-1} to $4.2\cdot10^{-3}$ h^{-1} (from –12 to 42 units on the chart), which agrees with the above estimates. The chart of frequency shifts is shown over a chart of the temperature at 300 m showing the dynamic structure in the region and locations of the eddies and northern periphery of the Kuroshio Current. Strong positive variations in the frequency of inertial oscillations are associated with the regions of anticyclonic vorticity determined by the mesoscale eddy and Kuroshio Current. Note the large positive values of frequency shift in the region of the anticyclonic eddy centered at 40°N, 153°E and in the southern part of the region, which reaches the northern boundary of the Kuroshio Current. A shift of 10 units (0.001 cyc/hour $\approx 3\cdot10^{-7}$ s^{-1}) corresponds to almost half-hour variation in the inertial period.

Part of the *Megapolygon* study region was occupied by a warm anticyclonic eddy with negative vorticity of the same sign as the vorticity of inertial oscillations. Vorticity associated with the eddy can be estimated from the frequency shift of near-inertial waves in the region occupied by the eddy. The shift of frequency in the eddy average over the measurements on 15 moorings results in vorticity $\xi \sim 3.4\cdot10^{-3}$ h^{-1}, while the maximum estimated vorticity is $\xi \sim 8.2\cdot10^{-3}$ h^{-1}. This vorticity corresponds to a horizontal velocity shear of a few centimeters per second (2–5 cm/s) over 20 kilometers, which is an appropriate estimate for anticyclonic eddy.

9. Conclusions

We have provided solid experimental arguments to show that the response of the ocean to hurricane propagation manifests in the deep propagation of near-inertial, internal waves. However, their generation is not uniform over the region influenced by the hurricane and, as expected, depends on the local properties of the ocean, such as stratification and vorticity. The amplitudes of near-inertial, internal waves are greater in the regions of negative vorticity (clockwise motion) and near a strong current. Thus, the energies of eddies and currents enhance inertial oscillations. Our results support Munk's idea (1980) that the fine structure of the inertial peak can be approximated by an Airy function.

Mean anticyclonic vorticity in the region increases the effective frequency of near-inertial, internal waves by 0.001–0.004 cyc/hour.

Immediate generation of near-inertial, internal waves occurs in the entire water column due to a sharp atmospheric pressure jump. Later, strong winds induce surface perturbations and shear, which generate near-inertial, internal waves that propagate slowly downwards. The velocity of their propagation varies in the range 1–10 m/hour in the upper layers, increasing to 30 m/hour in the abyssal depths. Wind-generated, near-inertial, internal waves reach a depth of 1200 m (where many current meters were located) in a few days after the hurricane passes the region.

In the regions of low stratification and high anticyclonic vorticity, the velocity of downward propagation of near-inertial, internal waves increases.

The amplitudes of near-inertial, internal waves generally decrease with depth as the signal propagates downwards.

The near-inertial, internal waves generated by a hurricane last up to 10–12 days after which they reach the background level or a new wave packet arrives.

Acknowledgements

The visit of the first author (EGM) to the Instituto Pluridisciplinar, UCM, was made possible by a Visitor's Grant from the BSCH-UCM Program. The research was also supported by the NWO-RFBR Program, Grant No. 047.017.2006.003.

References

Abramowitz, M. and I. A. Stegun (eds.) (1972): *Handbook of Mathematical Functions with Formulas, Graphs, and Mathematical Tables* (Sect. 10.4). Dover, New York.

Alford, M. H. (2001): Internal swell generation: the spatial distribution of energy flux from the wind to mixed layer near-inertial motions. *J. Phys. Oceanogr.*, **31**, 2359–2368.

Balmforth, N. J., S. G. Llewellyn Smith and W. R. Young (1998): Enhanced dispersion of near-inertial waves in an idealized geostrophic flow. *J. Mar. Res.*, **56**, 1–40.

Blackman, R. B. and J. W. Tukey (1958): *The Measurements of Power Spectra from the Point of View of Communications Engineering*. Dover, New York.

Brink, K. H. (1989): Observations of the response of thermocline currents to a hurricane. *J. Phys. Oceanogr.*, **19**, 1017–1022.

Brooks, D. A. (1983): The wake of hurricane Allen in the western Gulf of Mexico. *J. Phys. Oceanogr.*, **13**, 117–129.

Church, J. A., T. M. Joyce and J. M. Price (1989): Current and density observations across the wake of hurricane Gay. *J. Phys. Oceanogr.*, **19**, 259–265.

D'Asaro, E. A. and H. Perkins (1984): A near-inertial wave spectrum for the Sargasso Sea in late summer. *J. Phys. Oceanogr.*, **14**, 489–505.

Fu, L.-L. (1981): Observations and models of internal waves in the deep ocean. *Rev. Geophys. Space Phys.*, **19**, 141–170.

Garrett, C. (2001): What is the "near-inertial" band and why is it different from the rest of the internal wave spectrum? *J. Phys. Oceanogr.*, **31**, 962–971.

Gill, A. E. (1984): On the behavior of internal waves in the wakes of storms. *J. Phys. Oceanogr.*, **14**, 1129–1151.

Healey, D. and P. H. LeBlond (1969): Internal wave propagation normal to a geostrophic current. *J. Mar. Res.*, **27**, 85–98.

Klein, P., S. Llewellyn Smith and G. Lapeyre (2004): Organization of near-inertial energy by an eddy field. *Quart. J. Roy. Meteor. Soc.*, **130**, issue 598, 1153–1166.

Kundu, P. K. (1984): Generation of coastal inertial oscillations by time-varying wind. *J. Phys. Oceanogr.*, **14**, 1901–1913.

Kunze, E. (1985): Near-inertial wave propagation in geostrophic shear. *J. Phys. Oceanogr.*, **15**, 544–565.

Kunze, E. and E. Boss (1998): A model for vortex-trapped internal waves. *J. Phys. Oceanogr.*, **28**, 2104–2115.

Lozovatsky, I. D., E. G. Morozov and H. J. S. Fernando (2003): Spatial decay of energy density of tidal internal waves. *J. Geophys. Res.*, **108**(C6), 3201–3207.

Maeda, A., K. Uejima, T. Yamashiro, M. Sakurai, H. Ichikawa, M. Chaen, K. Taira and S. Mizuno (1996): Near-inertial motion excited by wind change in a margin of the thyphoon 9019. *J. Oceanogr.*, **52**, 375–388.

Mao, Q., S. W. Chang and R. L. Pfeffer (2000): Influence of large-scale initial oceanic mixed layer depth on tropical cyclones. *Mon. Wea. Rev.*, **128**, 4058–4070.

Maximenko, N. A., M. N. Koshlyakov, Yu. A. Ivanov, M. I. Yaremchuk and G. G. Panteleev (2001): Hydrophysical experiment "Megapolygon-87" in the northwestern Pacific Subarctic frontal zone. *J. Geophys. Res.*, **106**, 14143–14163.

Mooers, C. N. K. (1975): Several effects of a baroclinic current on the cross-stream propagation of inertial-inertial waves. *Geophys. Fluid Dyn.*, **6**, 245–275.

Morozov, E. G., K. Trulsen, M. G. Velarde and V. I. Vlasenko (2002): Internal tides in the Strait of Gibraltar. *J. Phys. Oceanogr.*, **32**, 3193–3206.

Morozov, E. G., G. Parrilla-Barrera, M. G. Velarde and A. D. Scherbinin (2003): The straits of Gibraltar and Kara Gates: a comparison of internal tides. *Oceanol. Acta*, **26**, 231–241.

Munk, W. (1980): Internal wave spectra at the buoyant and inertial frequencies. *J. Phys. Oceanogr.*, **10**, 1718–1728.

Munk, W. and N. Phillips (1968): Coherence and band structure of inertial motion in the sea. *Rev. Geophys.*, **6**, 447–472.

Nilsson, J. (1995): Energy flux from traveling hurricanes to the internal wave field. *J. Phys. Oceanogr.*, **25**, 558–573.

Parks, T. W. and C. S. Burrus (1987): *Digital Filter Design* (Sect. 7.3.3). Wiley, New York.

Pedlosky, J. (1987): *Geophysical Fluid Dynamics* (Sect. 2.7). Springer Verlag, New York.

Pinkel, R. (1984): Doppler sonar observations of internal waves: the wavenumber frequency spectrum. *J. Phys. Oceanogr.*, **14**, 1249–1270.

Pollard, R. T. (1970): On the generation by winds of inertial waves in the ocean. *Deep-Sea Res.*, **17**, 795–812.

Pollard, R. T. (1980): Properties of near-surface inertial oscillations. *J. Phys. Oceanogr.*, **10**, 385–398.

Price, J. F. (1981): Upper ocean response to a hurricane. *J. Phys. Oceanogr.*, **11**, 153–175.

Price, J. F., T. B. Sanford and G. Z. Forristal (1994): Forced stage response to a moving hurricane. *J. Phys. Oceanogr.*, **24**, 233–260.

Qi, H., R. A. de Szoeke, C. A. Paulson and C. C. Eriksen (1995): The structure of near-inertial waves during ocean storms. *J. Phys. Oceanogr.*, **25**, 2853–2871.

Sanford, T. B., P. G. Black, J. R. Haustein, J. W. Feeney, G. Z. Forristall and J. F. Price (1987): Ocean response to a hurricane, Part. 1, Observations. *J. Phys. Oceanogr.*, **17**, 2065–2083.

Shay, L. K. and R. L. Elsberry (1987): Near-inertial ocean current response to hurricane Frederic. *J. Phys. Oceanogr.*, **17**, 1249–1269.

Shay, L. K., S. W. Chang and R. L. Elsberry (1990): Free surface effects on the near-inertial ocean response to a hurricane. *J. Phys. Oceanogr.*, **20**, 1405–1424.

Shay, L. K., G. J. Goni and P. G. Black (2000): Effects of a warm oceanic feature on hurricane Opal. *Mon. Wea. Rev.*, **128**, 1366–1383.

Taira, K., S. Kitagawa, H. Otobe and A. Tomio (1993): Observation of temperature and velocity from a surface buoy moored in the Shikoku Basin (OMLET-88)—an oceanic response to a typhoon. *J. Oceanogr.*, **49**, 397–406.

Treguier, A. M. and P. Klein (1994): Instability of wind-forced inertial oscillations. *J. Fluid Mech.*, **275**, 323–349.

van Meurs, P. (1998): Interactions between near-inertial mixed layer currents and the mesoscale: The importance of spatial variabilities in the vorticity field. *J. Phys. Oceanogr.*, **28**, 1363–1368.

Young, W. R. and M. Ben Jelloul (1997): Propagation of near-inertial oscillations through a geostrophic flow. *J. Mar. Res.*, **55**, 735–766.